The Astrophysical Journal, 775:135 (7pp), 2013 October 1 doi:10.1088/0004-637X/775/2/135

SWIFT OBSERVATIONS OF 1FGL J1018.6−5856

Hongjun An[1], François Dufour[1], Victoria M. Kaspi[1,3], and Fiona A. Harrison[2]
[1] Department of Physics, McGill University, Rutherford Physics Building, Montreal, QC H3A 2T8, Canada
[2] Cahill Center for Astronomy and Astrophysics, California Institute of Technology, Pasadena, CA 91125, USA
Received 2013 May 28; accepted 2013 August 7; published 2013 September 16

ABSTRACT

We report on X-ray properties of the gamma-ray binary 1FGL J1018.6−5856 using observations obtained with the *Swift* X-ray telescope. Using 54 observations made between MJD 55575 and 55984, we find that the X-ray flux is modulated at a period of 16.57 ± 0.11 days, which is consistent with previous reports based on gamma-ray data. We find that the X-ray maximum at phase 0 previously reported may not be a persistent feature of the source: the dramatic increases at phase 0 were only detected for ∼100 days and were not detected thereafter. Rather, the persistent sinusoidal maximum seems to be at phase 0.3–0.4, and is misaligned with the gamma-ray (GeV) peak. We also find evidence that the source's X-ray flux is correlated with the spectral hardness in the 0.5–10 keV band. Such a correlation has also been reported in the gamma-ray binaries LS 5039 and LS I +61°303 and can help us to understand the X-ray emission mechanisms of the sources.

Key words: binaries: close – gamma rays: stars – stars: individual (1FGL J1018.6−5856) – X-rays: binaries

Online-only material: color figures

1. INTRODUCTION

Gamma-ray binaries are a subclass of binary systems in which persistent GeV and/or TeV gamma rays are observed. They are composed of a massive stellar companion and a compact source, and emit photons in wide range of frequencies, from the radio to the very high energy (TeV) gamma-ray band. Although a firm classification is still missing for some sources, we list the known gamma-ray binaries in Table 1 (see Mirabel 2012 for a review). The origin of the gamma rays is a key puzzle in these sources.

There are two main models for the gamma-ray emission from these sources: microquasar models (see Bosch-Ramon & Khangulyan 2009 for review) and pulsar models (see Torres 2011 for review). In the former, gamma rays are suggested to be produced in jets by Compton upscattering of the stellar UV photons (e.g., Kaufman-Bernadó et al. 2002; Dubus et al. 2010) or hadronic decay (e.g., Romero et al. 2003). In the latter, gamma rays are produced by emission from accelerated pulsar wind particles in the shock between the pulsar and the stellar wind (e.g., Tavani et al. 1994; Tavani & Arons 1997; Dubus 2006), or from Compton upscattering of the stellar photons by the pulsar wind particles in the pulsar wind zone (e.g., Sierpowska-Bartoski & Torres 2008). While these models give general descriptions of the gamma-ray emission from the gamma-ray binaries, some sources show peculiar behavior (e.g., dramatic and periodic radio outbursts and magnetar-like bursts from LS I +61°303; Harrison et al. 2000; Barthelmy et al. 2008; De Pasquale et al. 2008; Burrows et al. 2012) which is not presently well understood in any model (e.g., Martí & Paredes 1995; Torres et al. 2012).

The 0.5–10 keV X-rays are thought to be produced via the synchrotron or the inverse Compton process by the shock-accelerated electrons or via accretion onto the compact object. In the wind interaction model (Tavani et al. 1994; Tavani & Arons 1997), the X-ray flux and spectrum are expected to vary with orbital phase. The details strongly depend on the orbital geometry and the mass loss rate of the stellar companion (see Dubus 2006; Chernyakova et al. 2006; Bogovalov et al. 2008; Takata et al. 2012 for recent developments). Nevertheless, Tavani & Arons (1997) suggest that the temporal behavior of the X-ray flux and spectrum is the best diagnostic for the wind interaction models. Therefore, accurately measuring the X-ray properties of gamma-ray binaries is important to test the models and to understand the physical processes in the systems.

Ackermann et al. (2012) discovered significant gamma-ray and X-ray modulation from the gamma-ray binary 1FGL J1018.6−5856 at a period of 16.58 ± 0.02 days. They noted that the orbital modulation of the X-ray and gamma-ray flux and the spectral variability of the gamma rays over the orbital period are similar to those seen in LS 5039 in general, but different in detail. The optical counterpart was spectroscopically classified as O6V((f)) using the South African Astronomical Observatory 1.9 m telescope and the 2.5 m telescope at Las Campanas Observatory (Ackermann et al. 2012), however, the orbital parameters of the system are not yet well known.

Here, we report on the X-ray properties of 1FGL J1018.6−5856 using the *Swift* X-Ray Telescope (XRT). We find that the X-ray flux varies with a period of 16.57 ± 0.11 days, which is consistent with the gamma-ray-measured value. Furthermore, we show evidence that the X-ray hardness is correlated with the 0.5–10 keV flux. We compare our results with those of other gamma-ray binaries whose compact object is (or is assumed to be) a pulsar.

2. OBSERVATIONS

We used 54 *Swift* XRT observations obtained from 2011 January 14 to 2012 February 27 (MJD 55575–55984), one 20 ks *XMM-Newton* observation (full frame mode) in 2008 October (MJD 55066), and one 10 ks *Chandra* (TE full frame mode) observation in 2010 August 17 (MJD 55425). The 54 *Swift* XRT observations (all in PC mode) had different exposures ranging from ∼0.7 ks to ∼10 ks.

We processed the *Swift* observations with `xrtpipeline` along with HEASARC remote CALDB,[4] using the standard

[3] Lorne Trottier Chair; Canada Research Chair.

[4] http://heasarc.nasa.gov/docs/heasarc/caldb/caldb_remote_access.html

Table 1
Properties of the Known Gamma-Ray Binaries

Source	Detected[a]	P_{orb} (days)	e[b]	Compact Source[c]	Companion	Γ_X[d]	Corr.[e]	References
1FGL J1018.6−5856	R, X, G	16.58	...	Pulsar?	O6V((f))	1.44–1.96[f]	Yes	1, 2, 3
LS 5039	R, X, G, T	3.9	0.35	Pulsar?	O6.5V((f))	1.45–1.61	Yes	4, 5, 6, 7
LS I +61°303	R, X, G, T	26.5	0.55	Pulsar?	Be	1.7–2.0	Yes	8, 9, 10, 11
PSR B1259−63	R, X, G, T	∼1240	0.9	Pulsar	Be	1.35–1.83	No	12, 13, 14, 15
Cyg X-3	R, X, G, T	0.2	...	Black hole?	Wolf-Rayet	... [g]	No	16, 17, 18
HESS J0632+057	R, X, T	321	...	Pulsar?	B0pe	1.2–1.6	No	19, 20, 21, 22

Notes.
[a] Detected energy band. R = Radio, X = X-ray, G = GeV gamma ray, T = TeV gamma ray.
[b] Orbital eccentricity.
[c] Question mark if unconfirmed.
[d] Power-law photon index in the ∼0.5–10 keV band.
[e] Anti-correlation between flux and photon index in the ∼0.5–10 keV band.
[f] Without five flares. See text for more details.
[g] Continuum is not modeled with a power law.
References. (1) Ackermann et al. 2012; (2) Li et al. 2011a; (3) Abramowski et al. 2012; (4) Paredes et al. 2000; (5) Takahashi et al. 2009; (6) Abdo et al. 2009a; (7) Aharonian et al. 2006; (8) Abdo et al. 2009b; (9) Li et al. 2011b; (10) Albert et al. 2006; (11) Harrison et al. 2000; (12) Tam et al. 2011; (13) Aharonian et al. 2005; (14) Johnston et al. 1992; (15) Kaspi et al. 1995; (16) Watanabe et al. 1994; (17) Abdo et al. 2009c; (18) Sinitsyna et al. 2011; (19) Hinton et al. 2009; (20) Skilton et al. 2009; (21) Bongiorno et al. 2011; (22) Rea & Torres 2011. See also references therein.

filtering procedure (Capalbi et al. 2005) to produce cleaned event files. In each cleaned event file, we found 3–246 events within a 20″ radius centered on the source position. The first 30 observations were analyzed and reported by Ackermann et al. (2012). However, we reanalyzed them for consistency.

For the *XMM-Newton* data, we processed the observation data files with `epproc` and `emproc` and then applied the standard filtering procedure (e.g., flare rejection and pattern selection) of Science Analysis System (SAS) version 11.0.0.[5]

The *Chandra* data were reprocessed using `chandra_repro` of CIAO 4.4 along with CALDB 4.4.7 so that we use the most recent calibration files. They are used for the imaging analysis only because a meaningful spectral analysis was impossible due to pile-up.

3. DATA ANALYSIS AND RESULTS

3.1. Imaging Analysis

We detected the source in the 10 ks *Chandra* data using `wavdetect` and found the source position to be R.A. = $10^h18^m55^s.62$ and decl. = $-58°56'46''.06$. This is consistent with what was reported by Ackermann et al. (2012) using *Swift* UVOT, the United States Naval Observatory B1.0 catalog, and radio observations made with the Australia Telescope Compact Array: R.A. = $10^h18^m55^s.60$, decl. = $-58°56'46''.2$, (J2000). We then searched for point sources that may contaminate the *Swift* or *XMM-Newton* spectra in a circular region (radius = 90″). We found none, which validates the extraction regions that we use below.

We also checked whether the *XMM-Newton*- and *Swift*-measured positions were consistent with the known position using `edetect_chain` and `wavdetect`, respectively. The positions we found agreed with the known one within the uncertainties, except for in one *Swift* observation where the source was offset by ∼9″ (2σ). The latter offset in a single observation is to be expected given the large number of observations. Note that `wavdetect` did not detect the source in four *Swift* observations for which the number of counts within a 20″ radius was less than 10. We ignored these observations in the analyses below.

3.2. Timing Analysis

To search for pulsations, we first applied the barycenter correction to the events using `barycen` and `barycorr` for the *XMM-Newton* and the *Swift* event files, respectively. We then extracted photon arrival times from the event files.

Since the source is a binary, Doppler shifting of the pulsations could broaden a periodogram made assuming a fixed periodicity, which could reduce or entirely eliminate our sensitivity to pulses. We consider the effects of binary orbital Doppler shifting under the assumption of a circular orbit with 30° inclination. This assumption is reasonable because the eccentricity and inclination of 1FGL J1018.6−5856 are estimated to be low when we assume that the gamma rays are being produced via the inverse Compton process (Ackermann et al. 2012). Furthermore, we assume the mass of the secondary star to be 25 $M_\odot$ (see Puls et al. 1996 for example) and the primary star to be 1.4 $M_\odot$ (for a neutron star). For the known orbital period (16.58 days), we find that the orbital speed of the primary star would be ∼240–250 km s^{-1}. In this case, the Doppler shift in the putative pulse period is $(\Delta P/P) \sim 4 \times 10^{-4}$ (i.e., $\sim 6 \times 10^{-9}$ s for a 20 ks observation for the minimum searching period of $P \sim 150$ ms). This is smaller than the independent period bins (e.g., $P^2/T \sim 1 \times 10^{-6}$ s for $P = 150$ ms and $T = 20$ ks), and thus the blurring is not a concern for the individual observations. The Doppler shift over a full orbit could be as large as $\sim 6 \times 10^{-5}$ s (for $P = 150$ ms), hence precluding searching for pulsations by combining observations.

We searched for possible pulsations (in the 0.5–10 keV and 1–7 keV bands) from the source using the H test (de Jager et al. 1989) in the individual *Swift* and *XMM-Newton* time series over the periods from the Nyquist limit of each detector (5.2 s for MOS1 and MOS2, 146 ms for PN, 5 s for XRT) to 2000 s and found no significant pulsations. The most significant peak occurred at $P \simeq 179$ ms in the *XMM-Newton* data (0.5–10 keV). The probability of this peak occurring by chance was ∼8%. Since this peak was not significant, we set an upper limit on the

[5] http://xmm.esac.esa.int/sas/

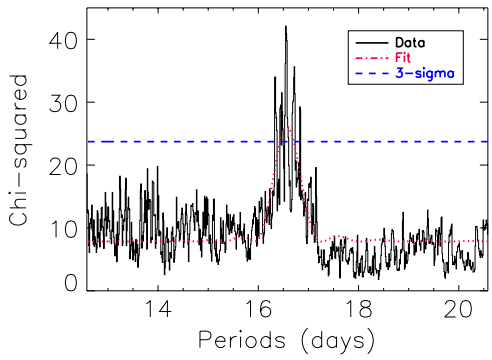

Figure 1. Chi-squared vs. period for the *Swift* X-ray data obtained using epoch folding (Leahy 1987) for a step size of 0.01 day with eight phase bins. The fit (red) gives the best period.

(A color version of this figure is available in the online journal.)

pulsed fraction to be $F_{\rm area} \lesssim 49\%$ or $F_{\rm rms} \lesssim 21\%$ with 90% confidence, where $F_{\rm area}$ and $F_{\rm rms}$ are defined as

$$F_{\rm area} = \frac{\sum_{i=1}^{N}(p_{i,\rm max} - p_{i,\rm min})}{\sum_{i=1}^{N} p_{i,\rm min}}$$

and

$$F_{\rm rms} = \frac{\sqrt{2\sum_{k=1}^{5}\left((a_k^2 + b_k^2) - (\sigma_{a_k}^2 + \sigma_{b_k}^2)\right)}}{a_0},$$

where $a_k = (1/N)\sum_{i=1}^{N} p_i \cos(2\pi ki/N)$, σ_{a_k} is the uncertainty in a_k, $b_k = (1/N)\sum_{i=1}^{N} p_i \sin(2\pi ki/N)$, σ_{b_k} is the uncertainty in b_k, p_i is counts in ith bin, and N is the total number of bins (see Gonzalez et al. 2010 for more details).

In order to measure the orbital period using the *Swift* data, we employed epoch folding (Leahy 1987), because it uses the count rates, and thus takes care of the highly unequal exposures of the observations. We folded the *Swift* light curves at different test periods around the *Fermi*-measured value (±4 days, step size = 0.01 days) with the phase fixed to zero at MJD 55403.3 (Ackermann et al. 2012). We found the best period to be $P_{\rm orb} = 16.57 \pm 0.11$ days, which is consistent with the *Fermi*-measured value (see Figure 1). We also tried different binnings (4–10 bins) and different step sizes (0.01–0.13 days) and found consistent results. We note that the detection significance was marginal ($\sim 3\sigma$, see Figure 1) even with the known period (no search trials), and thus it would have been very difficult to detect the X-ray modulation and measure the period without the guide of the gamma-ray measurement.

In Figures 2(a) and (b), we show the unfolded count rates as a function of time in days since the *Fermi* epoch (MJD 55403.3) and the count rates folded in orbital phase for each observation, respectively. We find that there is a sharp peak at phase ~0 as reported by Ackermann et al. (2012). To examine this in more detail, we select the five brightest fluxes and henceforth refer to them as "flares." We tried to measure the time scales for the flares by using various temporal binnings for each flare observation. We find no evidence that the flares occurred in a narrow time bin; rather, each of the flares seems to be longer

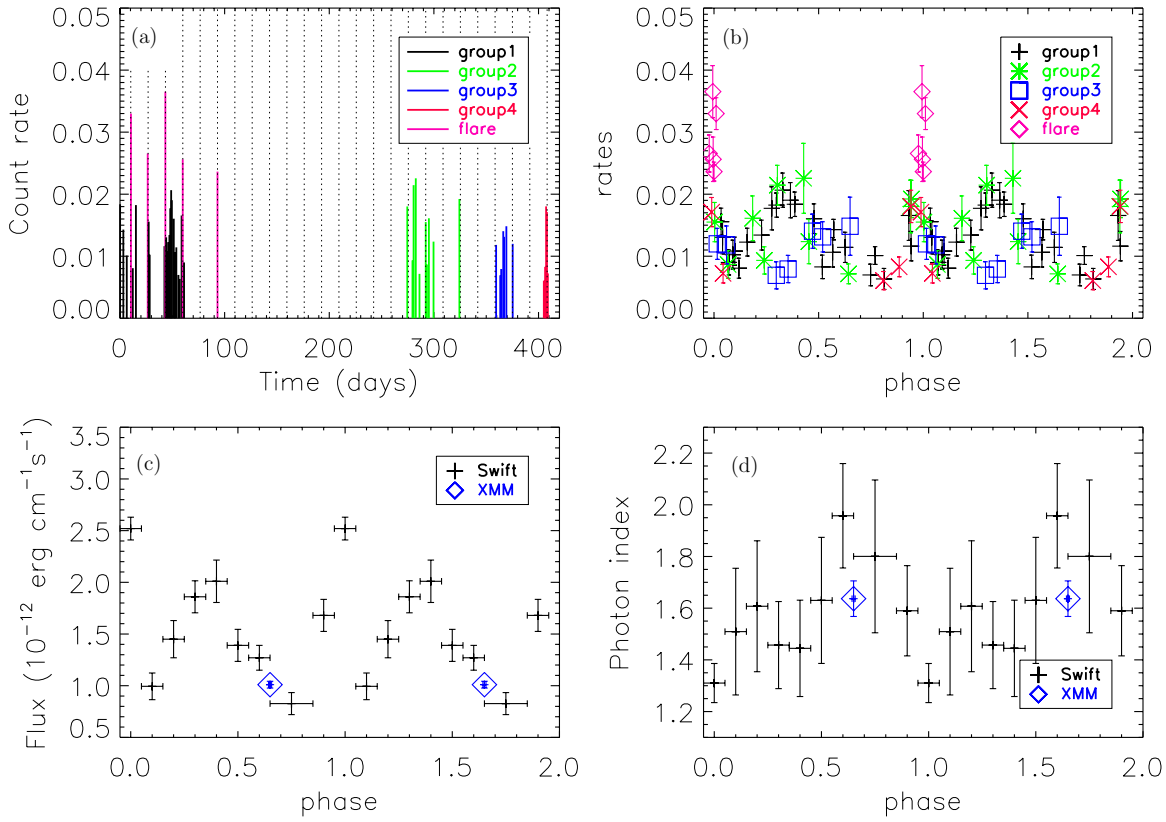

Figure 2. Observation times and count rates for *Swift* observations and the results of the spectral analysis. (a) Unfolded *Swift* light curve in the 0.5–10 keV band. The vertical dashed lines indicate phase 0. (b) *Swift* 0.5–10 keV count rates vs. orbital phase. (c) 0.5–10 keV absorption-corrected flux vs. orbital phase. (d) Power-law photon index vs. orbital phase.

(A color version of this figure is available in the online journal.)

Table 2
Summary of Spectral Fit Results

Phase[a]	Exposure (ks)	Counts[b]	N_H[c] (10^{22} cm^{-2})	Γ	Flux[d]	Method	Comment
0.65	20.0 (12.1[e])	2528	0.67(5)	1.64(7)	1.01(3)	χ^2	*XMM*
0	36.9	768	...	1.31(8)	2.52(11)	χ^2	*Swift* combined
1	12.3	115	...	1.51(25)	0.99(13)	cstat	*Swift* combined
2	7.9	98	...	1.61(25)	1.45(18)	cstat	*Swift* combined
3	14.2	203	...	1.46(17)	1.86(16)	χ^2	*Swift* combined
4	8.8	157	...	1.44(19)	2.01(21)	cstat	*Swift* combined
5	9.2	118	...	1.63(24)	1.40(15)	cstat	*Swift* combined
6	12.5	143	...	1.96(20)	1.27(12)	cstat	*Swift* combined
7–8	12.2	97	...	1.80(30)	0.73(11)	cstat	*Swift* combined
9	12.1	175	...	1.59(17)	1.68(15)	cstat	*Swift* combined
0[f]	22.1	582	...	1.30(9)	3.12(16)	χ^2	*Swift* combined
0[g]	14.7	193	...	1.50(16)	1.49(13)	cstat	*Swift* combined

Notes. Uncertainties are at the 1σ level.
[a] Orbital phase as reported by Ackermann et al. (2012).
[b] Within the extraction regions and in the 0.5–10 keV. MOS1, MOS2, and PN combined for *XMM*.
[c] N_H was measured with the *XMM-Newton* data and fixed to 0.67×10^{22} cm^{-2} for the *Swift* data fits.
[d] Absorption-corrected flux in the 0.5–10 keV band in units of 10^{-12} erg cm^{-2} s^{-1}.
[e] For PN detector.
[f] The five flares in Figures 2(a) and (b).
[g] Without the five flares.

than the observations (2–10 ks). We note that large flares like those that occurred in the first ∼100 days of the observations were not observed in groups 2, 3, and 4 in spite of exposure at phase 0 in all three groups (see Figures 2(a) and (b)).

We note that there are two low outliers at phase ∼0.3–0.4 in group 3 (blue in Figure 2(b)). For the 2 outliers, 11 and 13 events were collected in the source region (see Section 3.3) for 1.4 ks and 1.6 ks exposures, respectively. We checked if the photon collecting areas were reduced for the two observations due to bad pixels in the source region, but found no significant reduction. Therefore, we included them in the timing and spectral analyses.

3.3. Spectral Analysis

For the *Swift* data, we extracted the source spectra from a radius 20″ and the backgrounds from an annular region of inner radius 40″ and outer radius 80″ centered on the source position. For the observation in which the source position was offset by ∼9″ compared with the *Chandra* position, we shifted the source extraction region by that amount. The corresponding ARFs were produced using `xrtmkarf` and corrected for exposure using `xrtexpomap`. Each spectrum had ∼10–250 counts in it, but not all of the individual spectra were useful for a meaningful analysis. We folded the observations using 10 phase bins and the *Fermi* ephemeris because the latter is more precise than that measured in this work (see Section 3.2). We then combined the observations in each phase bin for the spectral analysis. Even after combining spectra, there were not enough events in some phases. Therefore, we had to further combine orbital phase bins 7 and 8 (see Table 2).

For the *XMM-Newton* data, we extracted the source spectrum from circular regions with a radius of 16″ and background spectra from source-free regions with a radius of 32″ on the same chip. Corresponding response files were produced using the `rmfgen` and `arfgen` tasks of SAS 11.0.0. The spectrum was then grouped to have a minimum of 20 counts per bin.

We used `XSPEC` 12.7.1 to fit the spectra. First, we fit the *XMM-Newton* data (MOS1, MOS2, and PN) with a simple absorbed power-law (`tbabs*pow`), an absorbed blackbody (`tbabs*bbody`), and an absorbed thermal bremsstrahlung model (`tbabs*bremss`). The power-law and the bremsstrahlung models fit the spectrum well (χ^2/dof = 95.87/120, 97.00/120, respectively), and the residuals from the fit were featureless. Although both the power-law and the bremsstrahlung models were acceptable, we report the power-law model, since it gives a slightly better fit and is more commonly used for other similar binary systems. The power-law fit parameters we obtained for the *XMM-Newton* data are consistent with the previously reported values (Pavlov et al. 2011; Abramowski et al. 2012).

For the *Swift* data, we attempted to fit the spectra using the usual chi-squared statistics. However, when there were insufficient events, we used the *C* statistic implemented as `cstat` in `XSPEC` without binning the spectrum (in the 0.5–10 keV band). We checked if the C-statistic fit results are comparable to the χ^2 results for two *Swift* observations that have enough counts (phases 0 and 3, see Table 2), and find that they agree within the statistical uncertainties. We fit the data with an absorbed power-law model.

Due to the paucity of counts, we could not measure the hydrogen column density (N_H) well for each orbital phase. However, we find that the N_H values measured with (1) the archival *XMM-Newton* observation (see Table 2) and (2) the *Swift* spectrum at phase 0, which is separated by ∼2 yr from the *XMM-Newton* observation, are consistent with each other, although the uncertainty in the *Swift* value of N_H was relatively large. Note that only 6%–10% of the variation in N_H has been seen in similar sources over a long period (e.g., LS 5039 and PSR B1259−63; Takahashi et al. 2009; Uchiyama et al. 2009). Furthermore, large orbital variations in N_H have only been seen in accreting systems (e.g., Miller et al. 2009), whereas 1FGL J1018.6−5856 shows no evidence of accretion (e.g., shows no features in its spectrum). Therefore, we fixed the value of N_H to that measured with *XMM-Newton*. The fit results are summarized in Table 2 and plotted in Figure 2(d).

In Figures 2(b) and (c), we see the phase 0 flux flares reported by Ackermann et al. (2012), but only in the first 100 days of

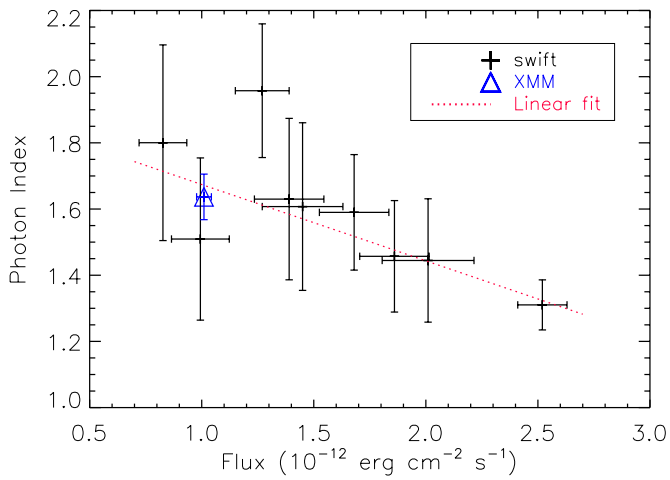

Figure 3. Correlation between 0.5–10 keV flux and photon index.
(A color version of this figure is available in the online journal.)

observations. To understand the properties of the flares (the five brightest points), we fit the combined spectrum of the flares (noted as "flare" in Figures 2(a) and (b)) and compare it with that of the remaining data in the same phase bin. For the flares, the combined spectrum was well fitted with an absorbed power law with a photon index of 1.30(9) and the flux was $3.12(16) \times 10^{-12}$ erg cm^{-2} s^{-1}. For the rest of the data in phase 0, the photon index was 1.50(16) and the flux was $1.49(13) \times 10^{-12}$ erg cm^{-2} s^{-1}. The very hard spectrum in phase 0 seems to be driven by the five flares, since those contain most of the events, and both of the separated spectra (five flares and the rest) in phase 0 seem to fit in the hardness/flux correlation trend individually (see Figure 3 and below). However, we note that the difference in the photon indexes is not statistically significant.

We find evidence of a negative correlation between the flux and the spectral hardness (see Figures 2(c) and (d), and 3). In order to quantify the significance of the putative correlation, we calculated the Spearman's rank order correlation coefficient. The rank order coefficient was $r_s = -0.77$ ($r_p = -0.71$ for Pearson's product–moment correlation coefficient) for 10 data samples, implying $\sim 3.4\sigma$ ($\sim 2.4\sigma$) significance for the (linear) correlation. If we ignore phase 0 where the flaring activity dominates the persistent emission (i.e., in case the flares are caused by a different physical process), then the correlation coefficient is $r_s = -0.68$ ($r_p = -0.63$), implying $\sim 2.5\sigma$ ($\sim 1.5\sigma$) significance.

We then conducted simulations to account for the uncertainties in the flux and photon index for the correlation. We first verified that the error contours for both parameters were approximately elliptical Gaussian. Since the parameters co-vary, we used the covariance matrices obtained during the spectral fits to properly account for this effect in our simulations. For each simulation, we varied the flux and photon index using Gaussian random numbers, calculated the rank order correlation coefficient, and counted the occurrences of non-negative correlation. The latter occurred 365 times in 10,000 simulations, suggesting that the confidence level of the negative correlation is $\sim$96% ($\sim$90% if we ignore phase 0).

We also tried to fit the data to a constant function (e.g., no correlation) or a linear function (e.g., negative correlation), taking into account both the uncertainties in the flux and the photon indices (Figure 3). The null hypothesis probability for the constant function was $\sim$5% (χ^2/dof = 16.9/9), and adding a linear slope improved the fit significantly (F-test probability of 0.001). The linear fit was acceptable with a null hypothesis probability of 86% (χ^2/dof = 3.9/8), and we measured the slope to be -0.23 ± 0.07 (per 10^{-12} erg cm^{-2} s^{-1}). We therefore conclude that there is evidence of anti-correlation between the spectral index and the flux but that additional data will be required to verify it.

4. DISCUSSION

We find that the X-ray flux of 1FGL J1018.6−5856 shows orbital modulation and evidence of being correlated with spectral hardness. We also find that the period of the X-ray orbital modulation is 16.57 ± 0.11 days, which is consistent with that of the gamma-ray modulation. Furthermore, we find that the average X-ray orbital light curve is smoother than previously reported, but is punctuated by occasional high-flux "flares" near orbital phase 0, and that the persistent peak of the orbital modulation in the X-ray flux appears to be in the phase 0.3–0.4.

1FGL J1018.6−5856 shares some X-ray properties with known gamma-ray binaries LS 5039, LS I +61°303, and PSR B1259−63, where the compact star companion is either known or generally assumed to be a neutron star. The photon index of 1FGL J1018.6−5856 in the 0.5–10 keV band varies between $\sim$1.3 and $\sim$2.0. These values and this range are similar to those of the other sources. Orbital variations of the photon index for other gamma-ray binaries are 1.45–1.61 for LS 5039 (Takahashi et al. 2009), 1.35–1.83 for PSR B1259−63 (Kaspi et al. 1995; Hirayama et al. 1999; Uchiyama et al. 2009), and 1.7–2.0 for LS I +61°303 (Li et al. 2011b). Spectral variation with orbital phase is expected in models of gamma-ray binaries, since any orbital eccentricity results in a varying separation between compact object and companion star, along with a variable relative shock distance and particle/photon flux at the shock location (e.g., Tavani et al. 1994; Tavani & Arons 1997; Dubus 2006; Bogovalov et al. 2008). In such models, we naively expect the spectral variability to be more pronounced for a source with large eccentricity. Indeed, the orbital variation of the spectral photon index is stronger for larger eccentricity in the case of the three sources, LS 5039, LS I +61°303, and PSR B1259−63 in Table 1. However, 1FGL J1018.6−5856 does not follow this trend; it has been argued that its eccentricity is small (Ackermann et al. 2012) but its spectral variation is large, which is puzzling. However, the current measurements have large uncertainties, and so they require verification with more precise measurements before we draw our final conclusions. We note that shock viewing geometry could also play a role in variable flux and spectral parameters, even in a circular orbit.

We find that the spectral index of 1FGL J1018.6−5856 shows evidence of being anti-correlated with the 0.5–10 keV flux (see Figure 3). The same trend was also observed in two of the gamma-ray binaries above (LS I +61°303 and LS 5039; Li et al. 2011b; Takahashi et al. 2009), but not in PSR B1259−63 (Kaspi et al. 1995; Hirayama et al. 1999; Uchiyama et al. 2009). It is puzzling that such a correlation should be present in some systems but not all, if indeed they all have a common nature.

Tavani et al. (1994) and Tavani & Arons (1997) proposed a pulsar wind/stellar wind interaction model for PSR B1259−63. In the model, the locations of the termination shock as a function of the orbital phases are determined by the orbital geometry and pressure balance of the two winds. The time scales of various physical processes (e.g., particle acceleration,

the synchrotron radiation, and the inverse Compton processes) and spectral parameters are then calculated. Tavani & Arons (1997) noted that different interaction models can be best tested using the time behavior of the X-ray luminosity and spectrum, and they demonstrated the X-ray flux and spectral variability with changing orbital phase for PSR B1259−63.

For 1FGL J1018.6−5856, the stellar wind outflow (for O6V star companion; Puls et al. 1996) may be larger than, but different in geometry from, that in PSR B1259−63 (which has a Be star companion), where the mass outflow rate is smaller but is more concentrated in the equatorial plane for the case of a Be star (Bjorkman & Cassinelli 1993). Considering this, the effective mass outflow parameter (Υ/f; Tavani et al. 1994) for an O6V star can be comparable to or larger than that of a Be star. In such a case, the model predicts that the dominant physical process would be synchrotron radiation, which is consistent with what we infer from the correlation between radio and X-ray flux below. Although it may be possible to apply the model to 1FGL J1018.6−5856 given a detailed orbital geometry, the orbital geometry is not yet constrained so detailed modeling cannot presently be done.

We note that our observed hardness/flux correlation cannot be due to orbital variation of $N_{\rm H}$. If it were, then one would expect the count rate to be smaller for a harder spectrum, which we do not observe. If we assume that $N_{\rm H}$ varies by as much as 10% for an orbit as has been seen in other gamma-ray binaries (e.g., LS 5039 and PSR B1259−63; Takahashi et al. 2009; Uchiyama et al. 2009), the variation can affect the photon index by ∼5%, which does not explain the much larger observed spectral variation.

Mirabel (2012) categorized gamma-ray binaries into three types based on their radiative behavior and the nature of the companion. According to the categorization, 1FGL J1018.6−5856 should be similar to LS 5039. Ackermann et al. (2012) argue that the two systems may differ based on the hardness/flux correlation in the gamma-ray band and the fact that the X-ray maximum coincides with the gamma-ray maximum for 1FGL J1018.6−5856 but not for LS 5039. However, we show that the large X-ray peak at phase 0 reported by Ackermann et al. (2012) is likely to be caused by occasional flaring behavior and is not obviously a persistent feature. The maximum of the sinusoidal modulation in the X-ray band lies at phase 0.3–0.4, which does not coincide with the 1–10 GeV gamma-ray peak (see Figure 4). Thus, the orbital phase offset between the X-ray (<10 keV) band and the gamma-ray band (1–10 GeV) is common to both 1FGL J1018.6−5856 and LS 5039.

We note that although the very bright "flares" previously reported near phase 0 for this source, in which the soft X-ray flux was seen to increase by factors of three to five, do not appear to be a persistent feature, some flux enhancement at that orbital phase is often present (see Figures 2(a) and (b)). Indeed, at phase 0, the X-ray flux is above the sinusoidal trend most of the time. However, no significant flux increase in the radio or hard X-ray band at this orbital phase has been observed (Ackermann et al. 2012; Li et al. 2011a). This is understandable if the flare amplitude during the radio and hard X-ray observations was small, and/or the observations did not sample the "narrow" flare phase well enough to make a sensitive detection of the flare. Nevertheless, the sinusoidal phases of the flux modulations in the radio, soft X-ray (<10 keV), and hard X-ray (18–40 keV) bands are relatively well aligned (see Figure 4), implying that they are all misaligned with the gamma-ray phase. The phase alignment between the radio and the X-ray band may imply

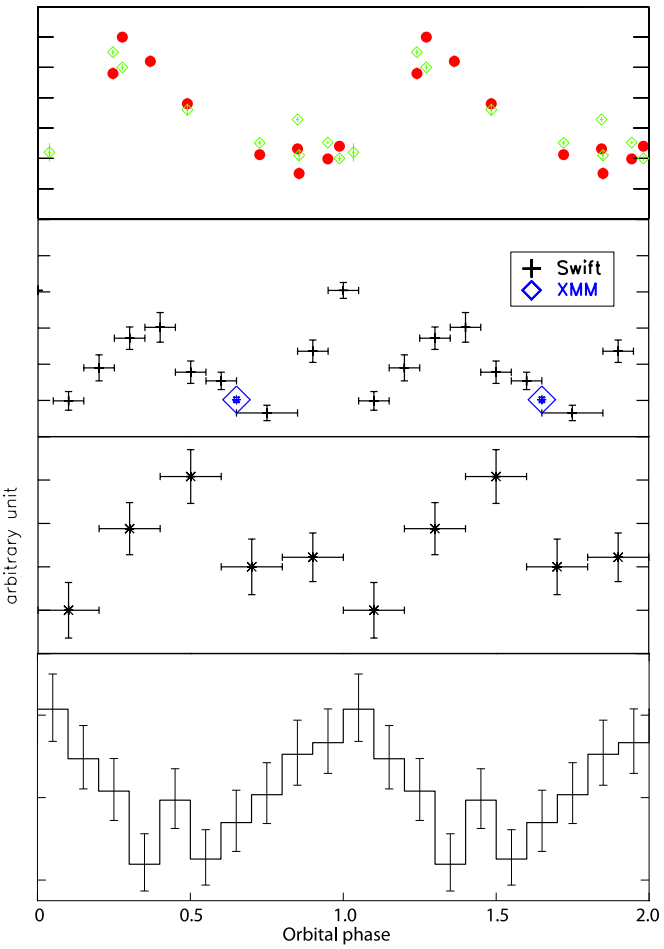

Figure 4. Orbital modulation of radio, X-ray, and gamma-ray fluxes. From top to bottom, the panels show the radio data (diamonds at 9 GHz and circles at 5.5 GHz, figure taken from Ackermann et al. 2012), 0.5–10 keV absorption-corrected flux (from this work), count rates in the 18–40 keV band (Li et al. 2011a), and 1–10 GeV flux (figure taken from Ackermann et al. 2012).

(A color version of this figure is available in the online journal.)

that the X-ray emission mechanism is a synchrotron process, unlike in LS I+61°303 where an offset between the radio and X-ray phases was observed, and the X-ray emission was suggested to be due to an inverse Compton process (Harrison et al. 2000).

Similar X-ray flares have also been seen in other systems (e.g., LS I+61°303 and LS 5039, Li et al. 2011b; Kishishita et al. 2009). The flares in LS I+61°303 are aperiodic with a kilosecond time scale (Li et al. 2011b), and those in LS 5039 seem to be periodic with a 10–20 ks time scale (Kishishita et al. 2009). Although we were not able to clearly characterize the time scale of the flares in 1FGL J1018.6−5856, they seem to be periodic and the duration is rather long (≳2–10 ks), similar to those of LS 5039 but with relatively larger amplitudes.

The two systems, 1FGL J1018.6−5856 and LS 5039, share many properties, such as a flux/hardness correlation in the soft X-ray band, phase alignment between the soft and the hard X-ray bands (Li et al. 2011a), and misalignment between the X-ray and GeV gamma-ray orbital phases. However, they show different flux/hardness correlations in the gamma-ray band. Detailed modeling and broadband observations in the future will help us to tell clearly whether or not the two systems are different in nature.

5. CONCLUSIONS

We have analyzed *Swift*, *XMM-Newton*, and *Chandra* data for the gamma-ray binary 1FGL J1018.6−5856, and we find the orbital period of the X-ray (<10 keV) flux to be 16.57 ± 0.11 days, which is consistent with the value measured in the gamma-ray band. We also show that the previously reported very large flux increase at phase 0 (factors of ∼3–5) occurred only for the first ∼100 days of the *Swift* observations, although substantial increases in flux (a factor of ⩽2) are seen frequently in that phase. The persistent maximum of the X-ray orbital modulation seems to occur at phase 0.3–0.4 and is significantly misaligned with the 1–10 GeV gamma-ray peak. Finally, we show evidence that 1FGL J1018.6−5856 exhibits a correlation between spectral hardness and the flux in the 0.5–10 keV band, which is common to several gamma-ray binaries and can hopefully be used to help us to understand the nature of X-ray emission from these interesting objects.

This research has made use of data obtained from the High Energy Astrophysics Science Archive Research Center (HEASARC), provided by NASA's Goddard Space Flight Center. V.M.K. acknowledges support from an NSERC Discovery Grant, the FQRNT Centre de Recherche Astrophysique du Québec, an R. Howard Webster Foundation Fellowship from the Canadian Institute for Advanced Research (CIFAR), the Canada Research Chairs Program, and the Lorne Trottier Chair in Astrophysics and Cosmology.

REFERENCES

Abdo, A. A., Ackermann, M., Ajello, M., et al. 2009a, ApJL, 706, L56
Abdo, A. A., Ackermann, M., Ajello, M., et al. 2009b, ApJL, 701, L123
Abdo, A. A., Ackermann, M., Ajello, M., et al. 2009c, Sci, 326, 1512
Abramowski, A., Acero, F., Aharonian, F., et al. 2012, A&A, 541, A5
Ackermann, M., Ajello, M., Ballet, J., et al. 2012, Sci, 335, 189
Aharonian, F., Akhperjanian, A. G., Aye, K.-M., et al. 2005, A&A, 442, 1
Aharonian, F., Akhperjanian, A. G., Bazer-Bachi, A. R., et al. 2006, A&A, 460, 743
Albert, J., Aliu, E., Anderhub, H., et al. 2006, Sci, 312, 1771
Barthelmy, S. D., Baumgartner, W., Cummings, J., et al. 2008, GCN, 8215, 1
Bjorkman, J. E., & Cassinelli, J. P. 1993, ApJ, 409, 429
Bogovalov, S. V., Khangulyan, D. V., Kolodoba, A. V., Ustyugova, G. V., & Aharonian, F. A. 2008, MNRAS, 387, 63
Bongiorno, S. D., Falcone, A. D., Stroth, M., et al. 2011, ApJL, 737, L11
Bosch-Ramon, V., & Khangulyan, D. 2009, IJMPD, 18, 347
Burrows, D. N., Chester, M. M., D'Elia, V., et al. 2012, GCN, 12914, 1
Capalbi, M., Perri, M., Saija, B., Tamburelli, F., & Angelini, L. 2005, The *Swift* XRT Data Reduction Guide, Technical Report 1.2, http://swift.gsfc.nasa.gov/analysis/xrt_swguide_v1_2.pdf
Chernyakova, M., Neronov, A., & Walter, R. 2006, MNRAS, 372, 1585
de Jager, O. C., Swanepoel, J. W. H., Raubenheimer, B. C., et al. 1989, A&A, 221, 180
De Pasquale, M., Bathelmy, S. D., Baumgartner, W. H., et al. 2008, GCN, 8209, 1
Dubus, G. 2006, A&A, 456, 801
Dubus, G., Cerutti, B., & Henri, G. 2010, MNRAS, 404, L55
Gonzalez, M. E., Dib, R., Kaspi, V. M., et al. 2010, ApJ, 716, 1345
Harrison, F. A., Ray, P. S., Leahy, D. A., Waltman, E. B., & Pooley, G. G. 2000, ApJ, 528, 454
Hinton, J. A., Skilton, J. L., Funk, S., et al. 2009, ApJL, 690, L101
Hirayama, M., Cominsky, L. R., Kaspi, V. M., et al. 1999, ApJ, 521, 718
Johnston, S., Manchester, R. N., Lyne, A. G., et al. 1992, ApJL, 387, L37
Kaspi, V. M., Tavani, M., Nagase, F., et al. 1995, ApJ, 453, 424
Kaufman-Bernadó, M. M., Romero, G. E., & Mirabel, I. F. 2002, A&A, 385, L10
Kishishita, T., Tanaka, T., Uchiyama, Y., & Takahashi, T. 2009, ApJL, 697, L1
Leahy, D. A. 1987, A&A, 180, 275
Li, J., Torres, D. F., Chen, Y., et al. 2011a, ApJL, 738, L31
Li, J., Torres, D. F., Zhang, S., et al. 2011b, ApJ, 733, 89
Martí, J., & Paredes, J. M. 1995, A&A, 298, 151
Miller, J. M., Cackett, E. M., & Reis, R. C. 2009, ApJL, 707, L77
Mirabel, I. F. 2012, Sci, 335, 13
Paredes, J. M., Martí, J., Ribó, M., & Massi, M. 2000, Sci, 288, 2340
Pavlov, G. G., Misanovic, Z., Kargaltsev, O., & Garmire, G. P. 2011, ATel, 3288
Puls, J., Kudritzki, R.-P., Herrero, A., et al. 1996, A&A, 305, 171
Rea, N., & Torres, D. F. 2011, ApJL, 737, L12
Romero, G. E., Torres, D. F., Kaufman-Bernadó, M. M., & Mirabel, I. F. 2003, A&A, 410, L1
Sierpowska-Bartoski, A., & Torres, D. F. 2008, APh, 20, 239
Sinitsyna, V. G., Nikolsky, S. I., Mirzafatikhov, R. M., & Sinitsyna, V. Y. 2011, BRASP, 73, 437
Skilton, J. L., Pandey-Pommier, M., Hinton, J. A., et al. 2009, MNRAS, 399, 317
Takahashi, T., Kishishita, T., Uchiyama, Y., et al. 2009, ApJ, 697, 592
Takata, J., Okazaki, A. T., Nagataki, S., et al. 2012, ApJ, 750, 70
Tam, P. H. T., Huang, R. H. H., Takata, J., et al. 2011, ApJL, 736, L10
Tavani, M., & Arons, J. 1997, ApJ, 477, 439
Tavani, M., Arons, J., & Kaspi, V. M. 1994, ApJL, 433, L37
Torres, D. F. 2011, in Proc. First Session of the Sant Cugat Forum on Astrophysics, High-Energy Emission from Pulsars and their Systems, ed. N. Rea & D. F. Torres (Berlin: Springer), 532
Torres, D. F., Rea, N., Esposito, P., et al. 2012, ApJ, 744, 106
Uchiyama, Y., Tanaka, T., Takahashi, T., Mori, K., & Nakazawa, K. 2009, ApJ, 698, 911
Watanabe, H., Kitamoto, S., Miyamoto, S., et al. 1994, ApJ, 433, 350